Journal of Earth Science, *Vol. 21*, *No. 1*, *p. 55–70*, *February 2010* *ISSN 1674-487X*
Printed in China
DOI: 10.1007/s12583-010-0005-4

Activity and Formation of Sand Waves on Northern South China Sea Shelf

Luan Xiwu* (栾锡武)
Key Laboratory of Marine Geology and Environment, *Institute of Oceanology*, *Chinese Academy of Sciences*, *Qingdao* 266071, *China*
Peng Xuechao (彭学超)
Guangzhou Marine Geological Survey, *Ministry of Land and Resources*, *Guangzhou* 510760, *China*
Wang Yingmin (王英民)
Basin and Reservoir Research Center, *Chna University of Petroleum*, *Beijing* 102249, *China*
Qiu Yan (邱燕)
Guangzhou Marine Geological Survey, *Ministry of Land and Resources*, *Guangzhou* 510760, *China*

ABSTRACT: Sand waves on the northern South China Sea shelf had been considered as stable relict bed form. For the industry use of sea bed between stations LF13-2 and LF13-1, a new round of explorations were conducted. The newly obtained data show that both spacings and amplitudes of sand waves are all systematically changing with water depth. Repeated observations since 2003 to 2004 showed that the sea bed is currently active. Due to strong erosion of surface sediment since Dongsha (东沙) uplifting, there are almost no modern sediments on the shelf of Dongsha area. Sand materials in the study area mainly originate from the erosion of the bed sediment formation. The water depth increment revealed by repeated echo sounder data is mainly due to erosion. Bottom currents are quite complex in the area of Dongsha underwater plateaus. At site 9MKII, the southward ebb current is stronger than the northward flood current, while at site AEM-HR, the WNW-ward flood current is slightly stronger than the ESE-ward ebb current. At site 9MKII, the maximum bottom current speed is 48 cm/s, and 22% of the observed bottom current speeds are larger than 20 cm/s, which meet the minimum bottom current speed required for the creation of sand wave. This article points out that present-day oceanographic condition couples well with the sand-wave morphologies, and that the sand waves are to a great extent in equilibrium with the ongoing present-day oceanographic bottom current condition and active.

KEY WORDS: sand wave, northern South China Sea shelf, activity, formation.

INTRODUCTION

As we have known for a long time, the sea floor is not entirely flat. In many areas, various bed forms occur (Knaapen et al., 2001). Among them, barchan dune is the most basic and most actively studied bed-form type (Todd, 2005). In planview, a submarine barchan dune is crescent in shape with a convex stoss slope, a concave lee slope, and two horns bending to the lee side (Sauermann et al., 2000; Hesp and Hastings, 1998) (Fig. 1). An idealized barchan dune shape

This study was supported by the National Basic Research Program of China (973 Program) (No. 2007CB411702), and the National Natural Science Foundation of China (Nos. 40572067, 40776032).

*Corresponding author: xluan@ms.qdio.ac.cn

Manuscript received June 20, 2009.
Manuscript accepted September 5, 2009.

is symmetrical with the two horns, but asymmetrical shapes are commonly introduced by variation in flow direction, changes in sand supply, inclined bed surfaces, and so on (Landcaster, 1982). The long gentle stoss slope indicates the direction of the upstream, while the short steep lee slope indicates the direction of the downstream. Sediment is transported as bed load along the stoss slope until it reaches the crest, where it tumbles down and deposits at the lee slope (Harris and Collins, 1984; McCave and Langhorne, 1982). In the case of symmetrical barchan dune, the flow direction coincides with the symmetrical axis and from the stoss side to the lee side. Water flow and sand supply are believed to be the key components for the formation and evolution of submarine barchan dune (Best, 2005; Venditti and Bauer, 2005; Best and Kostaschuk, 2002; Nelson et al., 1995). Empirical evidence suggests that as flow velocity increases, the barchan dune will ultimately alter its shape to sand ridge by enlarging its width and shortening its two horns, while as flow velocity decreases and the sand supply increases, the barchan dune will shorten its width, stretch and extend its horns, and ultimately alter its shape to sand wave (Livingstone et al., 2007; Hersen et al., 2004).

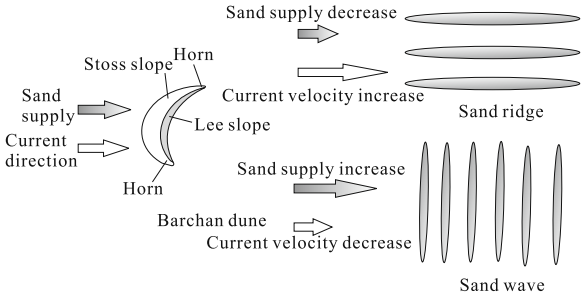

Figure 1. Schematic planview of the evolution of barchan dune, sand ridge, and sand wave (adapted from Sauemann et al., 2000; Hesp and Hastings, 1998).

Sand waves, not like isolated barchan dunes, are jointly rhythmic field features usually covering a large area on the sea floor. More than that, now, we know that sand waves are a dominant morphologic feature on most of the world continental shelf with water depth ranging from a few meters to several hundred meters (e.g., Dalrymple and Hoogendoorn, 1997; Trowbridge, 1995; McBride and Moslow, 1991; Swift and Field, 1981; Duane et al., 1972; Swift et al., 1972). Some of the sand waves are believed to be relic bed forms which were developed during the Last Glacial Maximum in a subaerial exposure environment or a coastal shallow water environment and emerged to its current depth after the transgression of rising sea level across the shelf (Todd, 2005), while some of the sand waves are active and in an equilibrium situation with the current hydrodynamic conditions (Todd, 2005). Active sand waves are very interesting from an engineering point of view because their migrating nature and long spatial and temporal scales may interfere with offshore activities. For instance, migrating sand waves may cause erosion, free spans of pipelines, and movement of seabed structures, possibly resulting in breakage of them (Todd, 2005; Nemeth et al., 2002; Meijdam and Lapidaire, 1995; Staub and Bijker, 1990). As the offshore activities are getting increasingly busy from the oil and gas development, the sand wave study becomes the key component of the systematic sea floor management. However, the activity of the sand waves has occupied considerable discussion and debate in literature (Goff et al., 1999).

GEOLOGICAL SETTING

The northern South China Sea shelf is the main part of northern South China Sea continental margin, bounded to the west by Vietnam, to the north by southeastern China mainland, and to the east by Taiwan Island, with two islands, namely, Hainan Island and Dongsha Islands, developed on it (Fig. 2).

Usually, the northern South China Sea shelf is referred to the part between Hainan and Taiwan, extending 900 km along the China mainland coast in the northeast direction and 300 km from Pearl River Mouth to the shelf break in the southeast direction, with Dongsha Islands as its outstanding feature in a generally flat and broad background. Dongsha Islands consist of two underwater plateaus. One of them is round in shape, situated at the shelf edge between 300-m and 600-m isobath lines, with an atoll emerging only a few tens of meters above the sea level. The other is 100 km northwest apart of the first one, quasi-rhombohedral in shape, elongated in the NE-SW direction, with three underwater shoals, namely, Lufeng, Beiwei, and Nanwei, distributed in the NE-SW direction (Fig. 3).

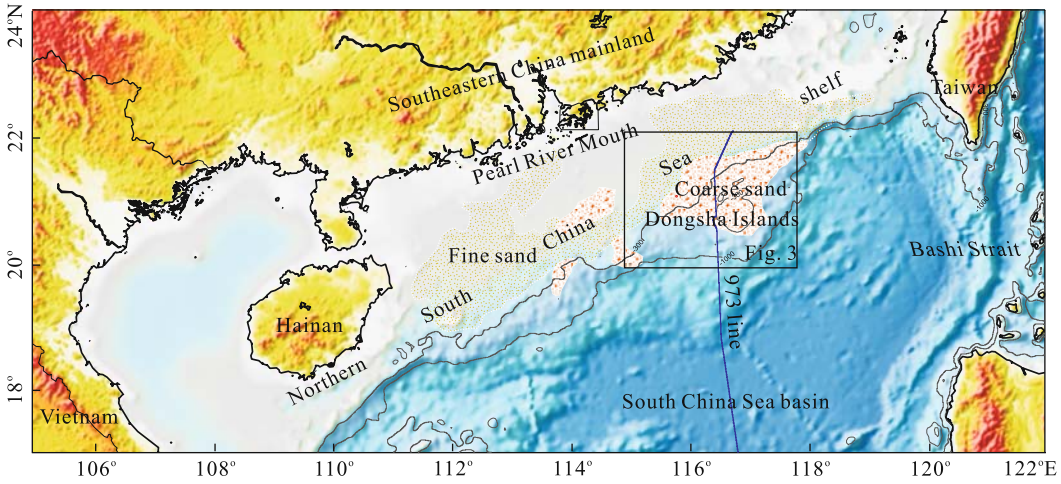

Figure 2. Map of northern South China Sea shelf.

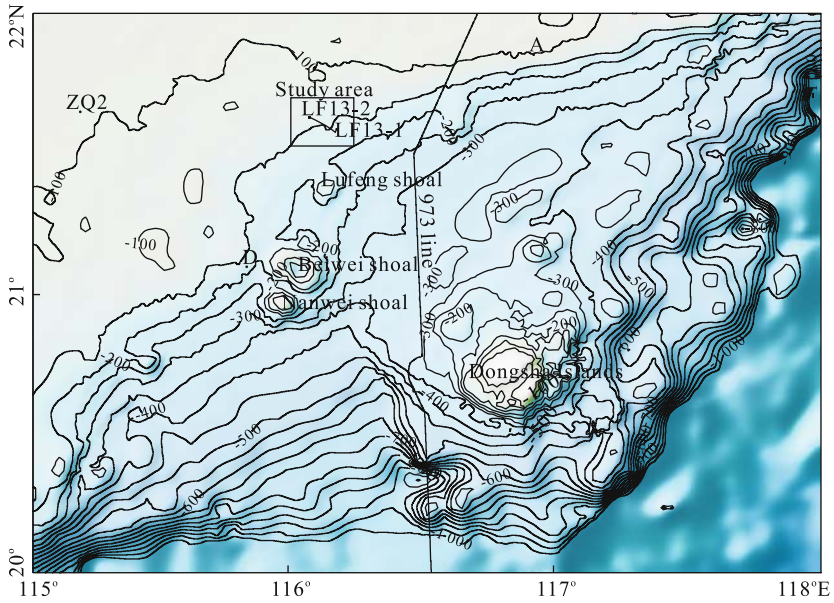

Figure 3. Dongsha underwater plateaus and the study area.

The water circulation pattern within the South China Sea is controlled by monsoons as well as by Kuroshio (Liang et al., 2003). During the summertime, the South China Sea warm current driven by the southwest monsoon flows northeastward along the shelf break of the northern South China Sea. During the wintertime, the South China Sea water masses, driven by northwest monsoon, flow southwestward (Wang et al., 1995; Shaw and Chao, 1994; Guan, 1993). The Kuroshio flow northward year-round along the east coasts of the Philippines and Taiwan Island. Along its way, part of the flow enters the South China Sea through the Bashi Strait, where it splits into two branches, one flowing into the East China Sea through the Taiwan Strait and the other forming a counter-clockwise current within the South China Sea. So the Kuroshio within South China Sea makes the summer current weaker and the winter current stronger.

At present, the Pearl River discharges approximately 300×10^9 m^3 of water and 90×10^6 t of sediment annually into the northern South China Sea shelf, and is considered as the main sediment source of the northern South China Sea shelf at present current regime (Gu et al., 1990). Though there are some articles believing that Changjiang River and Taiwan can also be sediment sources of the northern South China Sea shelf region (Liu et al., 2004; Zhang et al., 2003), other sources like Dongsha Islands were seldom considered.

The northern South China Sea shelf has been an

area of detailed investigations in the purpose of oil and gas exploration and production for many years. The results of marine geological work show that a large patch of fine sand exists in the middle shelf area between 50-m and 200-m isobath lines (Fig. 2). To the coastal area of southeastern China mainland, it changes to sandy clay and fine sandy clay, while to Dongsha Islands, it changes to coarse sand. Bed forms like sand wave had also been reported within the fine sand area. There was evidence that the South China Sea level had been down to 180 m during the Last Glacial Maximum and large part of its continental shelf exposed to the subaerial environment (Wang, 1999). Considering the sea-level change and also the carbon dating age of surface sediment sample, the fine sand was believed to be relict, and the sand wave was formed in the coastal or subaerial environment during the Last Glacial Maximum (Feng and Li, 1994).

For the industry use of sea bed between stations LF13-1 and LF13-2 (Fig. 3), a new round of geophysical, geological, and oceanographic explorations were conducted by Guangzhou Marine Geological Survey (GMGS) within the study area between LF13-2 and LF13-1 recently. In this article, we present the newly obtained geophysical and hydrodynamic data, and reexamine the activity and formation of the sand wave on the northern South China Sea shelf.

METHODOLOGY

The bed form data we used here were from two cruises. The first cruise was carried out on board of R/V Nanhai 503 from June 4, 2003 to July 4, 2003, hereafter called cruise 2003. The second cruise was carried out on board of R/V Fendou 4 from October 31, 2004 to November 3, 2004, hereafter called cruise 2004. The two cruises repeatedly surveyed the same area between LF31-2 and LF13-1.

Multibeam and side scan sonar were conducted on a survey net 1 000 m by 1 000 m at spacing of 100 m during cruise 2003. The SM-2000 system was used in the bathymetric mapping, while it was corrected by the compensator set near the transducer with an accuracy of ±10 cm. EG&G260 was used in the side scan sonar survey operating at a range of 150 m, with its tow fish kept at 80 m above seabed. The resolution of acquired side scan sonar data was around 30 cm.

The surface sediments and core sediments were collected with box sampler and gravity sampler, respectively, at sites B1, B2, B3, and B4 during cruise 2003 (Fig. 4).

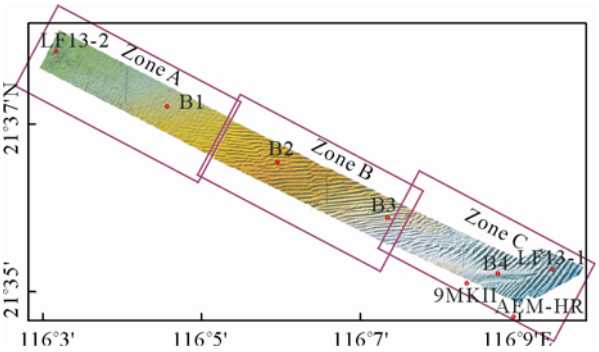

Figure 4. Multibeam results between LF31-2 and LF13-1.

During cruise 2004, multibeam and side scan sonar surveys were conducted with Simrad EM950 multibeam system and Klein 2000 side scan sonar, respectively. Merlin software was used to Simrad EM950 for field quality control. The accuracy of acquired multibeam bathymetry data was around 40 cm. The Klein 2000 side scan sonar was used with a maximum lateral range of 100 m, with data accuracy around 30 cm.

DGPS system was used during both cruise 2003 and cruise 2004. One delta fix radio link was utilized to provide differential corrections, while a DGPS receiver provided the raw GPS positions. Raw GPS positions and differential corrections were passed to navigation software and processed to get accurate positioning data. The accuracy has proven to be better than ±3 m.

The bottom current data we used here were from a summertime observation during July 28 to August 1, 2003 and a wintertime observation during 24 January to 9 March 2005 at site AEM-HR and site 9MKII, respectively (Fig. 4). The instruments were moored only a few meters above the sea floor to guarantee the bottom current observation.

Seismic data used in this article come from 973 Cruise by South China Sea Institute of Oceanology, Chinese Academy of Sciences in 2001 (Fig. 2). Seismic data were recorded at 2-ms sampling rate, 12-s record length by a 48-channel streamer with a group interval of 25 m. The energy source was an air-gun

array with a total volume of 0.02 m^3, shooting at an interval of 50 m (Li et al., 2008).

RESULTS

Topography and Geomorphology

Our primary observation derived from the multi-beam results is that the morphology within the survey area can be divided into three distinct zones based on sand wave development and orientation. We identify these zones as, from LF13-2 to LF13-1, zones A, B, and C. From Zone A to Zone C, the water depth changes gently from 130 to 145 m (Fig. 4).

Zone A

Zone A is near to LF13-2 and at the northwest sector of the survey area. The sea floor is basically flat in this zone, with slope of about 0.1% and dipping slightly from northwest at 129.9 m towards southeast to 132.7 m.

No distinct sand waves are observed in this zone. Locally pockmarks with dimensions of less than 10 m in diameter and 1 m in depth distribute randomly around LF13-2 (Fig. 4).

Zone B

Zone B is situated in the middle of Zone A and Zone C, with water depth between 132.7 and 140.1 m. The sea floor exhibits a flat topography with a very gentle regional slope of about 0.2% dipping from northwest to southeast.

Sand waves occur almost uniformly throughout this zone, with amplitudes systematically changing from 0.5 m in the northwest to 1.5 m in the southeast, and spacings (or widths, normal to crest strike) also systematically changing from 65 m in the northwest to 73 m in the southeast, and, again, its orientations (direction along sand wave crest) systematically changing from 93° in the north to 87° in the south.

Sand waves in this zone have straight or slightly straight crests, mainly showing as 2D bed forms. Along sand waves' crests, various variabilities like sand wave disappearance, direction changing, and forking can be found. The length of the sand waves' crests ranges from 800 m in the north to 1 350 m in the south. So there are more sand wave broken points in the northwest sector than in the southeast sector.

Most of the sand waves show asymmetrical cross-sections, with lee slopes directing roughly to the south and stoss slopes directing roughly to the north. The dipping slope of the lee side is usually 6%–8%, and the stoss side is around 2%–4%; that is, the slope of the stoss side approximately gets half the value of lee side (Berne et al., 1993; Langhorne, 1973).

Zone C

Zone C is near to LF13-1 and at the southwest sector of the survey area, located in water depths of between 140.1 and 145.1 m. The sea floor is basically flat with a gradient of about 0.3% dipping from northwest to southeast.

Sand waves occur throughout this zone, but with a more complex pattern. Two groups of sand waves can be found in this zone. Group 1 has its orientation roughly to the east, the same as that in Zone B. It's hard for us to give out the sand wave amplitude and spacing value of group 1 due to the modification by group 2. Sand waves of group 2 superimpose upon group 1, with orientation of 40°–50°, amplitude of 1–3 m, and spacing of 80–120 m.

In the area around LF13-1, sand waves of group 2 have also straight crests, mainly showing as 2D bed forms, and no sand wave broken points can be found. The length of the sand waves' crests is longer than 1 400 m. While in the area near to Zone B, where sand wave group 1 developed, sand wave group 2 mainly developed within the trough area between crests of sand wave group 1, showing 3D bed forms, with amplitude higher in the middle and narrowing and disappearing to the crests of sand wave group 1.

Sand wave group 2 also shows asymmetrical cross-sections, with lee slopes directing to the northwest, while the stoss slopes directing roughly to the southeast. The dipping slope of the lee side is roughly 8%, and the stoss side is around 3%; still, the slope of the stoss side approximately gets half the value of lee side (Berne et al., 1993; Langhorne, 1973).

No depressions with larger than 10 m in diameter exist in Zone B and Zone C.

There are some relationships between sand wave in Zone B and sand wave in Zone C. It seems that sand wave in Zone B did not disappear in Zone C, but was superimposed by another sand wave group in

Zone C and also evolved to it by gradually changing its orientation from 90° in Zone B to 45° in Zone C.

The correlation between sand wave formation and water depth has already been reported elsewhere on the world continental shelves (e.g., Stubblefield et al., 1984; Figueiredo et al., 1981; Swift and Field, 1981; Swift et al., 1972). Here in our study area, this correlation also exists clearly. Both amplitude and spacing of sand waves as described above increase with water depth from LF13-2 to LF13-1.

Sedimentary Facies

Sedimentary facies were investigated by surface and core sediments collection and combined by side scan sonar reflectivity. Surface and core sediments were collected at stations LF13-2, B1, B2, B3, B4, and LF13-1 by box sampler and gravity sampler, respectively, while side scan sonar survey was conducted within the whole study area.

Sediments at site LF13-2 are grayish green clayey silt, silty sand, and light greenish gray shelly sand. From LF13-2 through B1, B2, B3, B4, to LF13-1, the sedimentary types are various, mainly composed of clayey silt, sandy silt, silty sand with clay, silty sand, shelly sand, and gravel. Clay and silt contents of the sediments reduce from LF13-2 to LF13-1, while contents of sand and gravel of the sediments increase from LF13-2 down to LF13-1. The particle sizes of the sediments tend to change from fine at LF13-2 to medium at LF13-1, and the sediments become coarser from LF13-2 to LF13-1. The greenish color of the sediments is mainly due to content of organic matter. The organic matter contents are high in silty clay and clayey silt, and lower in sandy sediments. So, as the organic matter contents reduce from LF13-2 to LF13-1, the color of the sea floor sediments changes from grayish green to gray.

Side scan sonar reflectivity is commonly used in the surficial sedimentary face identification in conjunction with sea floor surface samples (Todd, 2005; Goff et al., 1999; Todd et al., 1999; Shaw et al., 1997; Mitchell and Hughes Clarke, 1994). A correspondence exists between side scan sonar reflectivity and surficial sediment roughness. Sea bed that constitutes mainly of clay and silt usually returns low reflectivity and is shown as white on the side scan sonar sonograms, while sea bed that constitutes of mainly sand returns high reflectivity and is shown as dark grey on the side scan sonar sonograms.

The side scan sonar records in the study area indicate that the sea bed is of generally uniform reflectivity and shows characteristics of silty to sandy sediments. The color of the recorded sonogram gently becomes darker from LF13-2 to LF13-1 (Fig. 5), which suggests that the sea floor sediment gently changes from finer at LF13-2 to coarser at LF13-1, which agrees well with the surface sediment collection results.

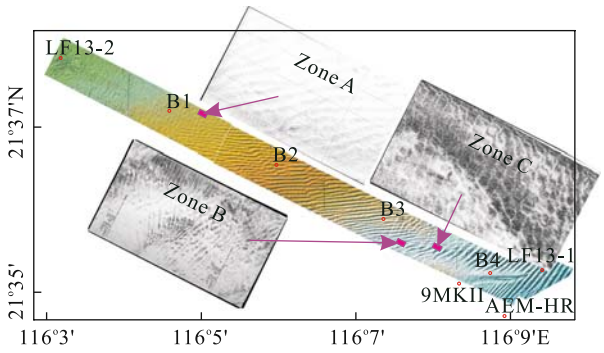

Figure 5. Side scan sonar sonogram of the study area.

Fine-scale bed forms clearly show on our side scan sonar sonogram results. In the north part in Zone A and Zone B, it mainly shows as sand ripple which is in the same pattern as sand wave with the same orientation but smaller amplitude and smaller spacing (Fig. 5). In Zone C, it shows a complex cellular pattern (Fig. 5), probably formed by two cross-cutting groups of sand ripples. All the fine-scale bed forms shown by the side scan sonar sonogram are superimposed on the sand waves shown by the multibeam results.

Sand Wave Movements

Echo sounder measurements had been conducted repeatedly between LF13-2 and LF13-1 during 2003 summer cruise and 2004 winter cruise. The time span between the two cruises is about 16 months, which is more than one year. The South China Sea is primarily controlled by the East Asian monsoon, characterized by seasonal switches in wind direction, precipitation, and runoff (Shaw and Chao, 1994; Webster, 1987). In addition, South China Sea is also subject to frequent

passage of typhoons, which also happens annually (Liu et al., 1998). So the data sets from those two cruises are an ideal material to examine the bed form activity which, on the most part, will be driven by East Asian monsoon and by typhoons if it is currently active.

To check the sand wave activity, echo sounder data sets from those two cruises had been carefully analyzed by tide corrections, system error removing, and so on. On the final results (Fig. 6), we do find bed form changes since summertime 2003 to wintertime 2004. First of all, the water depths systematically get deeper from LF31-2 to LF13-1 since summertime 2003 to wintertime 2004. In Zone A, little or no change can be found, while in Zone B, the average water depth increment can be 0.22 m; in Zone C, the water depth increment reaches 0.29 m (Fig. 6). Besides the water depth change, another obvious change is a newly born wave that appeared in Zone C at around 10.8 km from LF13-2 (Fig. 6). Sand wave movement can also be found. Around Zone B, the crests of sand waves of 2004 shift some time left hand and some time right hand, while they are all systematically getting lower than those of 2003. The offsets between crests of 2004 and 2003 are very small, usually within meters. Around Zone C, the crests of sand waves of 2004 shift left hand, while they are all systematically getting lower than those of 2003. That means the sand waves of 2004 had a northwestward movement as compared to those of 2003. The movement distance judged from the crest of 2004 to the crest of 2003 is around 8–13 m in Zone C.

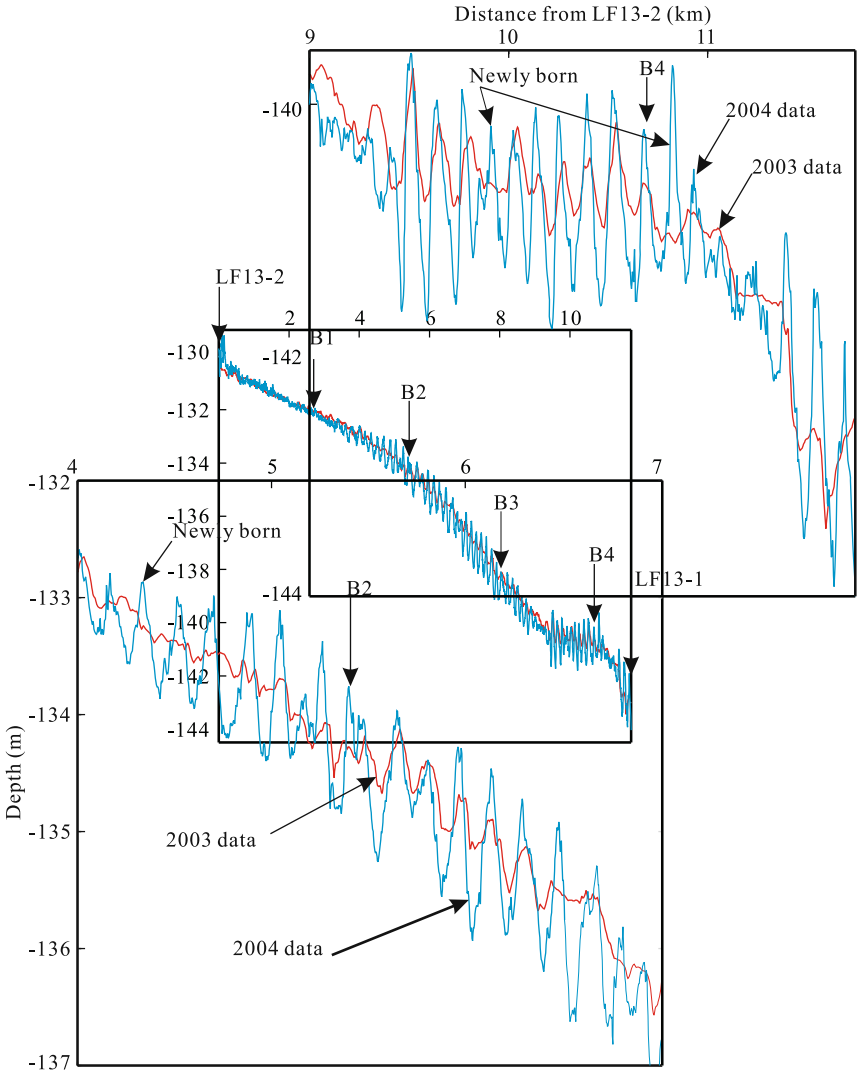

Figure 6. Sand wave change between summer 2003 and winter 2004.

Bottom Currents

To study the activity of submarine sand waves found on the northern South China Sea shelf, bottom current observation was carried out by Guangzhou Marine Geological Survey (GMGS) using an Underwater Buoy Current Observation System (RCM 9MKII Current Meter) in wintertime 2005. The RCM 9MKII Current Meter was placed 0.5 m above sea bed at site named 9MKII (116°8′20.1″E, 21°35′6.3″N) from January 24, 2005 until March 9, 2005. Amounts of 43 d and 2 101 groups of data were acquired at a sampling interval of 30 min.

The observed data are stable and smooth, and just have little saltation (unreasonable data). We eliminate those unreasonable data before analysis and replace them by the insert data. The observed bottom current speeds and directions are shown in Fig. 7.

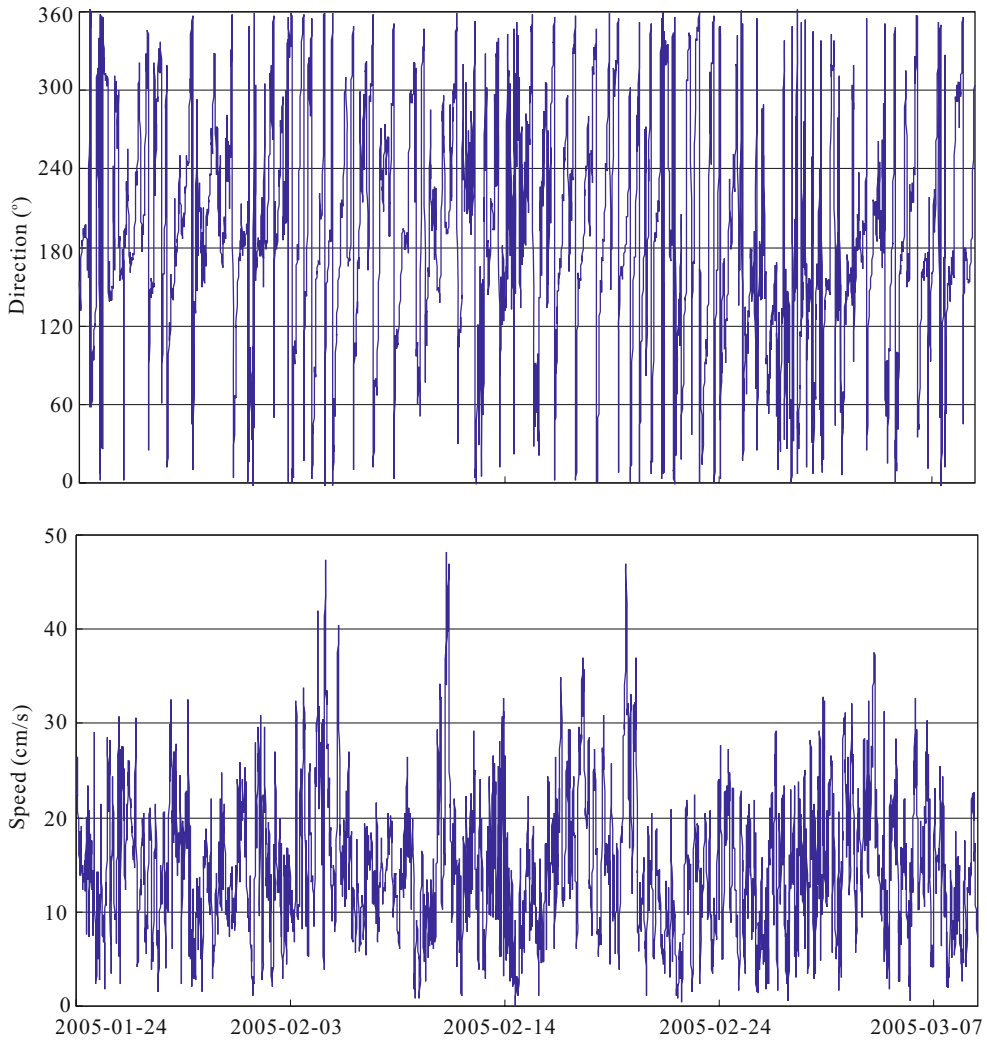

Figure 7. Bottom current speed and direction at site 9MKII from 24 Jan. 2005 to 9 Mar. 2005.

Among the 2 101 observed bottom current data, the maximum bottom current speed is 48 cm/s, and its direction is near to the south (190°), which happened at 11:00, Feb. 11, 2005, while the minimum bottom current speed is 0 cm/s, and its direction is near to the southwest (241°), which happened at 20:00, Feb. 14, 2005. The average bottom current speed is 15 cm/s; the main direction is SSE (165°–170°). 465 (around 22%) observed bottom current speeds are larger than 20 cm/s, 79 (around 4%) observed bottom current speeds are larger than 30 cm/s (Table 1), while only 13 (less than 1%) are larger than 40 cm/s.

Table 1 Observed bottom current data with speed larger than 30 cm/s from site 9MKII

No.	Date and time (y-m-d h:min)	Speed (cm/s)	Direction (°)	No.	Date and time (y-m-d h:min)	Speed (cm/s)	Direction (°)
1	2005-2-11 11:00	48.10	190.22	41	2005-2-11 04:30	32.85	167.01
2	2005-2-05 14:00	47.22	153.30	42	2005-3-01 18:30	32.85	18.99
3	2005-2-20 04:30	46.93	180.37	43	2005-1-29 02:00	32.56	139.94
4	2005-2-11 13:30	46.63	202.87	44	2005-2-11 04:00	32.56	161.03
5	2005-2-05 14:30	46.34	156.11	45	2005-3-06 05:30	32.56	214.12
6	2005-2-11 12:00	44.29	190.22	46	2005-1-29 22:00	32.26	326.28
7	2005-2-20 04:00	42.53	178.26	47	2005-2-04 04:00	32.26	172.28
8	2005-2-20 05:00	41.94	182.48	48	2005-2-20 14:30	32.26	165.96
9	2005-2-05 05:30	41.65	166.31	49	2005-3-01 19:30	32.26	9.14
10	2005-2-11 12:30	41.36	197.95	50	2005-1-29 02:30	31.97	148.02
11	2005-2-06 05:30	40.48	166.66	51	2005-2-05 04:30	31.97	169.82
12	2005-2-06 05:00	40.18	162.79	52	2005-2-05 15:30	31.97	166.66
13	2005-2-11 10:30	40.18	190.22	53	2005-2-14 05:00	31.97	163.14
14	2005-2-11 13:00	39.89	201.47	54	2005-2-20 06:30	31.97	203.93
15	2005-2-20 03:30	39.30	176.15	55	2005-3-03 03:00	31.97	159.63
16	2005-2-05 05:00	38.72	168.42	56	2005-3-03 23:30	31.97	349.14
17	2005-2-20 05:30	38.42	188.81	57	2005-2-05 06:30	31.68	201.47
18	2005-2-06 06:00	37.84	174.39	58	2005-2-18 01:00	31.68	168.77
19	2005-3-04 06:00	37.54	167.36	59	2005-2-20 13:00	31.68	146.97
20	2005-3-04 06:30	37.25	174.39	60	2005-2-17 00:30	31.38	164.20
21	2005-2-18 01:30	36.96	173.34	61	2005-3-06 06:00	31.38	214.48
22	2005-2-20 16:30	36.96	184.59	62	2005-2-14 06:00	31.09	155.76
23	2005-2-18 02:00	36.66	169.12	63	2005-2-17 00:00	31.09	166.66
24	2005-2-20 16:00	36.66	177.21	64	2005-2-20 06:00	31.09	203.22
25	2005-3-04 05:30	36.08	164.55	65	2005-3-02 19:30	31.09	60.48
26	2005-2-18 03:00	35.78	182.48	66	2005-1-26 13:00	30.80	160.68
27	2005-2-05 15:00	35.20	157.52	67	2005-2-02 10:30	30.80	180.72
28	2005-2-18 03:30	35.20	183.89	68	2005-2-14 04:00	30.80	131.50
29	2005-2-05 13:30	34.90	151.54	69	2005-2-18 02:30	30.80	180.72
30	2005-2-17 01:00	34.90	172.64	70	2005-2-19 03:00	30.80	184.59
31	2005-3-04 07:00	34.61	178.96	71	2005-2-20 15:30	30.80	172.64
32	2005-2-06 04:30	34.32	162.09	72	2005-3-04 17:30	30.80	165.96
33	2005-3-04 05:00	34.32	161.38	73	2005-1-27 08:30	30.50	297.81
34	2005-2-11 03:30	34.02	158.92	74	2005-2-04 04:30	30.50	170.53
35	2005-2-11 10:00	34.02	199.36	75	2005-3-02 18:00	30.50	10.20
36	2005-2-11 11:30	34.02	193.38	76	2005-2-04 12:00	30.21	123.06
37	2005-2-04 13:00	33.73	146.62	77	2005-2-05 10:30	30.21	355.82
38	2005-2-05 16:00	33.44	174.75	78	2005-2-11 09:30	30.21	195.84
39	2005-2-20 09:30	33.14	300.27	79	2005-3-06 19:30	30.21	159.63
40	2005-3-04 04:30	33.14	152.24				

The directions of bottom current with speed larger than 30 cm/s are quite concentrated (Fig. 8). Among the 79 observed bottom current data listed in Table 1, only 9 of them have their directions to the north or near to the north; for the rest, 70 have their directions to the south or near to the south, mostly concentrating within 165°–195°. From the higher speed (>30 cm/s) bottom current direction distributions, we can say that at site 9MKII, the south or near to the south ebb current is stronger than the north or near to the north flood current.

Based on the tidal current harmonic analysis, and according to the tidal current characteristics value, the current type in the investigated area belongs to irregular diurnal tidal current, and most of constituent currents rotate clockwise (Fig. 9). According to the tide observation, there are only one high water and one low water a day in most days, and there are two high waters and two low waters a day in a few days; a tide range of two high waters (or two low waters) is quite large. The tidal current changes along with tide quite well.

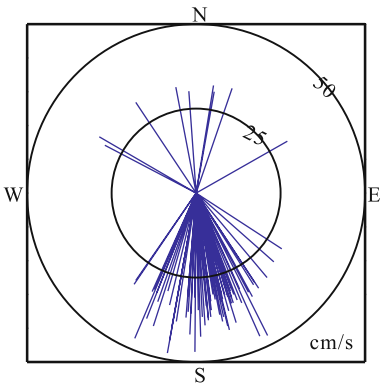

Figure 8. Rose map for the bottom current data with speed larger than 30 cm/s from site 9MKII.

Besides the wintertime bottom current observation, another short summertime bottom current observation was also carried out by GMGS in 2003 at a site about one thousand meters southeast to 9MKII. During this observation, AEM-HR Current Meter was used and placed about 5 m above sea bed at site named AME-HR (116°08′55.387″E, 21°34′42.729″N) from July 28, 2003 until August 1, 2003. About 5 d and 288 groups of data were acquired at a sampling interval of 20 min.

The observed data are reasonable and reliable. Among the 288 observed bottom current data, the maximum bottom current speed is only 15 cm/s, which is much smaller as compared to that observed during the wintertime, and its direction is also changed from south (190°) to east (95°), while the minimum bottom current speed is 5 cm/s, and its

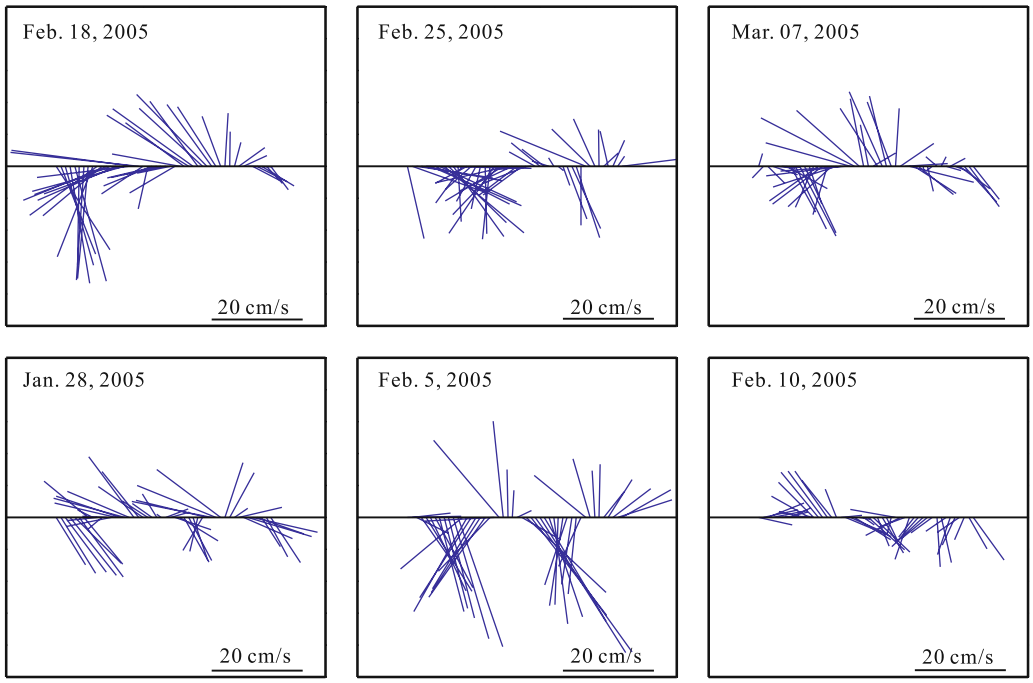

Figure 9. Bottom current observation results from site 9MKII.

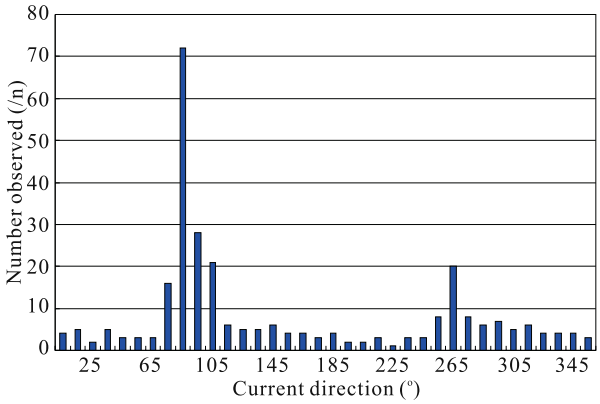

Figure 10. Statistics on the occurrence frequencies of observed bottom current in different directions at site AME-HR during 2003 summertime.

direction is near to the NNW (336°). The average bottom current speed is only 10 cm/s, which is also smaller than that observed during the wintertime. From the statistical result on the occurrence frequencies of observed bottom current in different directions (Fig. 10), we can say that, at site AME-HR during 2003 summertime, the main bottom current direction is on the east-west direction: around 50% of the whole 288 observed bottom currents direct to the east (70°–110°), and around 12% direct to the west (250°–280°), while the other directions averagely occupy 1%.

Based on the tidal current harmonic analysis, and according to the tidal current characteristics value, the current type at site AME-HR belongs to irregular diurnal tidal current, and most of constituent currents rotate clockwise. Diurnal constituent currents are stronger, and ellipticities are larger. The most possible direction of maximum bottom current speeds is to the west. It is shown from the maximum possible tidal current and tidal current frequency distributions that the WNW-ward flood current is slightly stronger than the ESE-ward ebb current.

DISCUSSION

Based on the experimental results and theoretical modal, Wang et al. (1990) gave out minimum bottom current speed for the movement of fine sand (grain size>0.075 mm), medium-fine sand (grain size>0.163 mm), and medium sand (grain size>0.25 mm) from sea bed as 19.8 cm/s, 29.2 cm/s, and 36.2 cm/s, respectively, and the minimum bottom current speed for the creation of sand waves on the sea bed as 23.6 cm/s, 34.7 cm/s, and 43.1 cm/s, respectively. Obviously, the northern South China Sea shelf present-day bottom currents, as shown by the observed results at stations 9MKII and AEM-HR, fall within the range of bottom current speed required for sediment movement and sand wave formation.

The northern South China Sea shelf is gently getting deeper from inner, middle shelves, to outer shelf, and the bathymetric contour lines on this area are usually uniform, except the area around Dongsha underwater plateaus (Fig. 3). Mainly due to the existence of Dongsha underwater plateaus, instead of uniform, parallel contour line distribution, the bathymetric contour lines in our study area are showing a complex pattern (Fig. 11), characterized by NE-paralleled contour lines in the northwest corner and EW-paralleled contour lines in the middle south corner, and, again, NE-paralleled contour lines in the eastern part. There is a mound feature (Lufeng shoal, Fig. 3) on the south boundary and a ridge feature 500 m west to site 9MKII (Fig. 11). The ridge feature stretches about 5 000 m long in north-south direction, about 500 m wide in east-west direction, and only 1–2 m high. The sand waves' distribution and arrangement in our study area present a good relationship with today's bathymetric contour lines and bed features. North to the mound feature and west to the ridge feature, the directions of sand wave crests are in east-west, which are parallel to the bathymetric contour lines. East to the ridge feature, the directions of sand wave crests are in northeast-southwest, which are also parallel to the bathymetric contour lines. The ridge feature serves as a boundary for both the sand wave pattern and the bathymetric contour line pattern. At this boundary, both the sand wave crests and bathymetric contour line change their directions.

Sand waves north to the Lufeng shoal, and west to the ridge feature, have their lee slopes directing roughly to the south and stoss slopes directing roughly to the north, while sand waves east to the ridge feature have their lee slopes directing roughly to the northwest and stoss slopes directing roughly to the southeast. The directions of lee slopes and stoss slopes of sand waves almost change oppositely while across the ridge feature from its west to its east. So the driven

flow patterns that created those sand wave asymmetries would definitely be different on each side of the ridge feature, considering the direct link between sand wave asymmetry and the driven flow (either wind for the subaerial environment or bottom current for the submarine environment) that created the sand wave (Ashley, 1990). If the sand waves in our study area were relict bed forms (Niino and Emery, 1961) created by wind due to subaerial exposure during the Last Glacial Maximum (Yim et al., 2006; Yim, 1999; Berry, 1959), it is hard to imagine that there would be two different wind regimes (Wang et al., 1999; Tchernia, 1980) existing over the study area, considering that the study area is only 10 km wide, and the ridge is only 1 m high.

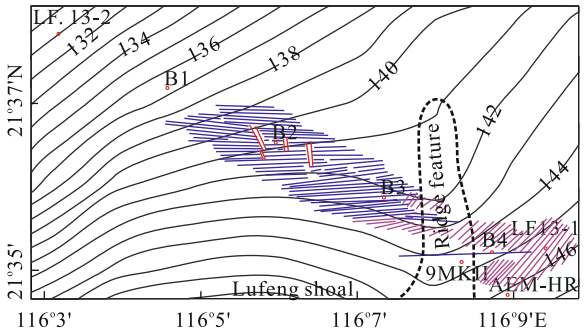

Figure 11. Relationship between sand wave directions and water depth contour lines.

Though we have no bottom current observation station west of the ridge feature in our sand wave area nearby sediment sampling station B2 or B3, deducing from the observation result of station 9MKII, we believe that the bottom current type west of the ridge feature area should belong to irregular diurnal tidal current, with stronger tidal current mainly directing to the southward and weaker ebb current directing to the north. So the present-day oceanographic condition couples well with the sand wave morphology. East to the ridge feature, based on the bottom current observation result from station AEM-HR, its present-day oceanographic condition, though different from that of the west of the ridge feature, also couples well with its sand wave morphology. Therefore, the sand wave morphologies are, to a great extent, in equilibrium with the ongoing present-day oceanographic bottom current conditions (Ikehara and Kinoshita, 1994) and mainly due to ongoing present-day oceanographic bottom current conditions.

Due to the uprising of Dongsha Islands, Dongsha underwater plateaus have a critical effect on the bottom current. Here in the study area, for the flood bottom current, it flows from the south and makes a left turn at the study area, and then flows to the north. While for the ebb bottom current, it flows from the north and again makes a left turn at the study area, and then to the south. Moreover, probably due to the water depth changing at the area of shelf break, gravity effect on the water column across the shelf break again makes the study area a critical position, allowing different oceanographic bottom current conditions coexist within our study area at present day, resulting a southward lee slope of sand wave west of the ridge feature and a northwestward lee slope of sand wave east of the ridge feature.

The coexistence of different oceanographic bottom current conditions in our study area probably is the key factor that controls the development of the superimposed sand waves in Zone C. So the superimposed sand waves in Zone C are another evidence for the modern formation of the sand waves, as Belderson et al. (1982) and Amos and King (1984) had already pointed out that relict sand waves do not have superimposed bed forms.

The sand wave spacings range from 65 to 130 m, less than two times water depth (292 m). According to Wang et al.'s (1990) bed-form classification, their formation environments should belong to deep water environment, other than coastal or subaerial environment.

The other evidence for the modern formation of the sand waves would be the correlation between sand wave parameters and water depth. As mentioned above, the amplitudes and spacings of our sand waves systematically change with water depth, while as have already reported by an existing article, this kind of correlation seldom exists for the relict sand wave (e.g., Stubblefield et al., 1984; Figueiredo et al., 1981; Swift and Field, 1981; Bowler, 1976; Swift et al., 1972).

The carbon dating ages of the surface sediment samples from stations around our study area belong to the Last Glacial Epoch (Feng and Li, 1994); for example, the age of station A was 15 ka, and the age of station D was 13 ka (Fig. 12; the locations of stations

A and D are shown in Fig. 3), which was an important factor for scientists to consider the sand waves as relict bed forms formed during the Last Glacial Epoch at the end of Pleistocene in a subaerial environment (Feng and Li, 1994). However, we argued that there are no modern sediments on middle and outer shelves of the northern South China Sea shelf around our study area due to strong erosion of surface sediment since the Dongsha movement (Li et al., 2008; Yan et al., 2006; Ludmann et al., 2001; Ludmann and Wong, 1999; Chen et al., 1987). Since the beginning of the Dongsha movement, magmatic intrusion had kept on uplifting and bending the sediment formations around the Dongsha area, causing a trough-like syncline structure north of Dongsha Islands with its hinge around the site LF13-1 (Fig. 12). So the sediment around the hinge of this syncline structure that is around LF13-1 should be the youngest around the Dongsha area. From the hinge to the south, the sediment will grow progressively older. A thin sheet of unsolidified sand coves on the solid bed, and it mainly originates from the erosion of the bed sediment formation (Fig. 12); a hard bed is helpful for the formation of sand wave fields (Le Bot and Trentesaux, 2004; Smith, 1988; Allen, 1984; Belderson et al., 1982).

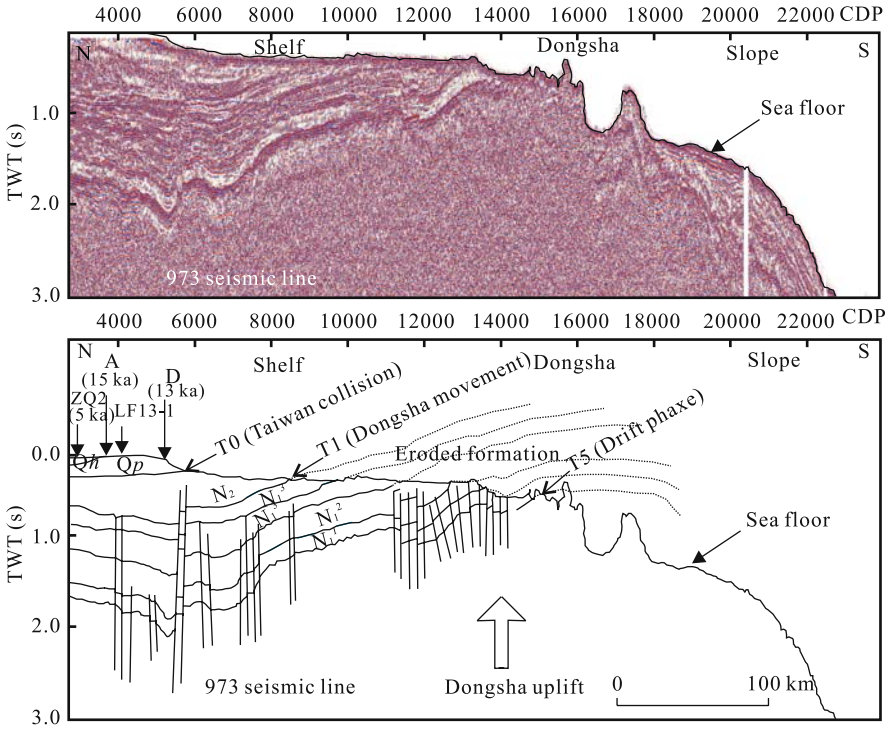

Figure 12. Eroded sediments redistributed on the shelf area after Dongsha movement.

CONCLUSIONS

Sand waves revealed by our multibeam data in our study area have straight or slightly straight crests, mainly showing as 2D bed forms, with both spacings and amplitudes systematically getting larger from northwest to southeast, and again, with its orientations changing from around 90° in the northwest to around 45° in the southeast. Sand waves in the northwest have their lee slopes directing roughly to the south, while sand waves in the southeast have their lee slopes directing to the northwest. They belong to two different systems of sand waves which superimpose upon one another, while both of them show clear relationship with water depth.

Besides the systematic change of sand wave with water depth, from LF13-2 to LF13-1, the surface sediment also changes systematically from fine to coarse, with sedimentary facies changing from clayey silt to shelly sand and gravel, particle sizes from fine to medium, and the sediment color from grayish green to gray.

Bed-form changing clearly exists since summer 2003 to winter 2004. Besides newly born waves and sand wave movement, a systematic water depth in-

crement also has been found. From LF13-2 to LF13-1, the year round increment can be as large as 0.29 m.

Due to strong erosion of surface sediment since the Dongsha movement, there are almost no modern sediments on middle and outer shelves of the northern South China Sea shelf around our study area. Sand materials in the sand wave area mainly originate from the erosion of the bed sediment formation. Year-round water depth increment revealed by echo sounder data is mainly due to this erosion.

Bottom currents are quite complex probably due to the development of Dongsha underwater plateaus. At site 9MKII, the southward ebb current is stronger than the northward flood current, while at site AEM-HR, the WNW-ward flood current is slightly stronger than the ESE-ward ebb current. At site 9MKII, the maximum bottom current speed is 48 cm/s, and 22% of the observed bottom current speeds are larger than 20 cm/s, which are near to the minimum bottom current speed required for the creation of sand wave on the sea bed. Obviously, the present-day oceanographic condition couples well with the sand wave morphologies, and the sand waves are, to a great extent, in equilibrium with the ongoing present-day oceanographic bottom current condition, and mainly due to ongoing present-day oceanographic bottom current conditions, they are active.

ACKNOWLEDGMENTS

The authors wish to thank the crew on R/V Nanhai 503 of Cruise 2003, the crew on R/V Fendou 4 of Cruise 2004, and also the crew on R/V Shiyan 2 of 2001 973 Cruise. This study was funded by the National Basic Research Program of China (973 Program) (No. 2007CB411702), and the National Natural Science Foundation of China (Nos. 40572067, 40776032).

REFERENCES CITED

Allen, J. R. L., 1984. Sedimentary Structures: Their Character and Physical Basis (Vol. 1). Elsevier, Amsterdam. 593

Amos, C. L., King, E. L., 1984. Bedforms of the Canadian Eastern Seaboard: A Comparison with Global Occurrences. *Mar. Geol*., 57: 167–208

Ashley, G. M., 1990. Classification of Large-Scale Subaqueous Bedforms: A New Look at an Old Problem. *J. Sedim. Petrol*., 60(1): 160–172

Belderson, R. H., Johnson, M. A., Kenyon, N. H., 1982. Bedforms. In: Stride, A. H., ed., Offshore Tidal Sands: Processes and Deposits. Chapman and Hall, London. 27–57

Berne, S., Castaing, P., Le Drezen, E., et al., 1993. Morphology, Internal Structure, and Reversal of Asymmetry of Large Subtidal Dunes in the Entrance to Gironde Estuary (France). *J. Sedim. Petrol*., 63(5): 780–793

Berry, L., 1959. Changing Sea Levels and Their Significance in Hong Kong. *Hong Kong University Engineering Journal*, 22: 23–34

Best, J. L., 2005. The Fluid Dynamics of Rivers: A Review and Some Future Research Directions. *Journal of Geophysical Research*, 110: F04S02

Best, J. L., Kostaschuk, R., 2002. An Experimental Study of Turbulent Flow over a Low-Angle Dune. *Journal of Geophysical Research*, 107: 3135–3154

Bowler, J. M., 1976. Aridity in Australia: Age, Origins and Expression in Aeolian Landforms and Sediments. *Earth-Science Reviews*, 12: 279–310

Chen, S., Li, Z., Zou, Y., 1987. Major Oil Accumulation Characteristics and Exploration Direction in the Pearl River Mouth Basin. *China Oil*, 4(4): 12–23

Dalrymple, R. W., Hoogendoorn, E. L., 1997. Erosion and Deposition on Migrating Shoreface-Attached Ridges, Sable Island, Eastern Canada. *Geosci. Can*., 24: 25–36

Duane, D. B., Field, M. E., Meisburger, E. P., et al., 1972. Linear Shoals on the Atlantic Inner Continental Shelf, Florida to Long Island. In: Swift, D. J. P., Duane, D. B., Pilkey, O. H., eds., Shelf Sediment Transport: Process and Pattern. Dowden, Hutchinson and Ross, Stroudsburg, Penn.. 447–498

Feng, W. K., Li, W., 1994. Seafloor Sand Waves in the Northern South China Sea. *Tropic Oceanology*, 13(3): 39–46 (in Chinese with English Abstract)

Figueiredo, A. G., Swift, D. J. P., Stubblefield, W. L., et al., 1981. Sand Ridges on the Inner Atlantic Shelf of North America: Morphometric Comparisons with Huthnance Stability Model. *Geo-Mar. Lett.*, 1: 187–191

Goff, J. A., Swift, D. J. P., Duncan, C. S., et al., 1999. High-Resolution Swath Sonar Investigation of Sand Ridge, Dune and Ribbon Morphology in the Offshore Environment of the New Jersey Margin. *Mar. Geol*., 161: 307–337

Gu, Q. S., Rao, K. Y., Li, X., et al., 1990. Remote Sensing Application in Lingdingyang Estuary. Science Press, Beijing (in Chinese with English Abstract)

Guan, B., 1993. Winter Counter-Wind Current off the Southeastern China Coast and Preliminary Investigation of Its Source. In: Su, J., Wen-Sin, C., Ya, H., eds., Proceedings of the Symposium on the Physical and Chemical Oceanography of the China Seas. Ocean Press, Beijing. 1–9

Harris, P. T., Collins, M. B., 1984. Side-Scan Sonar Investigation into Temporal Variation in Sandwave Morphology: Helwick Sands, Bristol Channel. *Geo-Mar. Lett*., 4: 91–97

Hersen, P., 2004. On the Crescentic Shape of Barchan Dunes. *European Physical Journal B*, 37: 507–514

Hesp, P. A., Hastings, K., 1998. Width, Height and Slope Relationships and Aerodynamic Maintenance of Barchans. *Geomorphology*, 22: 193–204

Ikehara, K., Kinoshita, Y., 1994. Distribution and Origin of Subaqueous Dunes on the Shelf of Japan. *Mar. Geol*., 120: 75–87

Knaapen, M. A. F., Hulscher, S. J. M. H., de Vriend, H. J., et al., 2001. A New Type of Bed Waves. *Geophysical Research Letters*, 28(7): 1323–1326

Lancaster, N., 1982. Dunes on the Skeleton Coast, SWA/Namibia: Geomorphology and Grain Size Relationships. *Earth Surface Processes and Landform*, 7: 575–587

Langhorne, D. N., 1973. A Sandwave Field in the Outer Thames Estuary, Great Britain. *Mar. Geol*., 14: 129–143

Le Bot, S., Trentesaux, A., 2004. Types of Internal Structure and External Morphology of Submarine Dunes under the Influence of Tide- and Wind-Driven Processes (Dover Strait, Northern France). *Mar. Geol*., 211: 143–168

Li, C., Zhou, Z., Hao, H., et al., 2008. Late Mesozoic Tectonic Structure and Evolution along the Present-Day Northeastern South China Sea Continental Margin. *Journal of Asian Earth Sciences*, 31(4–6): 546–561

Liang, W. D., Tang, T. Y., Yang, Y. J., et al., 2003. Upper-Ocean Currents around Taiwan. *Deep-Sea Res. II*, 50: 1085–1105

Liu, A. K., Chang, Y. S., Hsu, M. K., et al., 1998. Evolution of Nonlinear Internal Waves in the East and South China Seas. *Journal of Geophysical Research*, 103: 7995–8008

Liu, B. L., Wang, Y. P., Wang, J. Z., et al., 2004. Geochemical Characters of REE in the Seafloor Sediment in Northern Continental Slope of the South China Sea and Analysis of Source of Material and Diagenesis Environment. *Marine Geology & Quaternary Geology*, 24(4): 17–23 (in Chinese with English Abstract)

Livingstone, I., Wiggs, G. F. S., Weaver, C. M., 2007. Geomorphology of Desert Sand Dunes: A Review of Recent Progress. *Earth-Science Reviews*, 80: 239–257

Ludmann, T., Wong, H. K., 1999. Neotectonic Regime on the Passive Continental Margin of the Northern South China Sea. *Tectonophysics*, 311: 113–138

Ludmann, T., Wong, H. K., Wang, P., 2001. Plio-Quaternary Sedimentation Processes and Neotectonics of the Northern Continental Margin of the South China Sea. *Mar. Geol*., 172: 331–358

McBride, R. A., Moslow, T. F., 1991. Origin, Evolution and Distribution of Shoreface Sand Ridges, Atlantic Inner Shelf, USA. *Mar. Geol*., 97: 57–85

McCave, I. N., Langhorne, D. N., 1982. Sandwaves and Sediment Transport around the End of a Tidal Sandbank. *Sedimentology*, 29: 95–110

Meijdam, L., Lapidaire, P. J. M., 1995. Sandwaves, Upheaval Buckling Challenge North Sea Project. *Pipeline & Gas Industry*, 78: 31–38

Mitchell, N. C., Hughes Clarke, J. E., 1994. Classification of Sea Floor Geology Using Multibeam Sonar Data from the Scotian Shelf. *Mar. Geol*., 121: 143–160

Nelson, J. M., Shreve, R. L., McLean, S. R., et al., 1995. Role of Near-Bed Turbulence Structure in Bed Load Transport and Bed Form Mechanics. *Water Resources Research*, 31: 2071–2086

Nemeth, A. A., Hulscher, S. J. M. H., de Vriend, H. J., et al., 2002. Sand Wave Migration in Shallow Seas. *Continental Shelf Research*, 22(18–19): 2795–2806

Niino, H., Emery, K. O., 1961. Sediments of Shallow Portions of East China Sea and South China Sea. *Geological Society of America Bulletin*, 72: 731–762

Sauermann, G., Rognon, P., Poliakov, A., et al., 2000. The Shape of Barchan Dunes of Wouthern Morocco. *Geomorphology*, 36: 47–62

Shaw, J., Courtney, R. C., Currie, J. R., 1997. Marine Geology of St. George's Bay, Newfoundland, as Interpreted from Multibeam Bathymetry and Backscatter Data. *Geo-Mar. Lett*., 17: 188–194

Shaw, P. T., Chao, S. Y., 1994. Surface Circulation in the South China Sea. *Deep-Sea Res. I*, 41: 1663–1683

Smith, D. E., 1988. Morphological Development of the Sandettie South Falls Gas: A Degeneration Ebb Dominated Tidal Passage in the Southern North Sea. In: de Boer, P. L., Van Gelder, A., Nio, S. D., eds., Tide-Influenced Sedimentary Environments and Facies. D. Reidel Publishing, Utrecht. 51–64

Staub, C., Bijker, R., 1990. Dynamic Numerical Models for Sand Waves and Pipeline Self-Burial. In: Edge, B., ed.,

ICCE-Proceedings, ICCE. 2509–2521

Stubblefield, W. L., McGrail, D. W., Kersey, D. G., 1984. Recognition of Transgressive and Post-Transgressive Sand Ridges on the New Jersey Continental Shelf. In: Tillman, R. W., Siemers, C. T., eds., Siliciclastic Shelf Sediments. Soc. Econ. Paleontologists and Minerologists, Tulsa. 1–23

Swift, D. J. P., Field, M. E., 1981. Evolution of a Classic Sand Ridge Field: Maryland Sector, North American Inner Shelf. *Sedimentology*, 28: 461–482

Swift, D. J. P., Kofoed, J. W., Saulsbury, F. P., et al., 1972. Holocene Evolution of the Shelf Surface, Central and Southern Atlantic Shelf of North America. In: Swift, D. J. P., Duane, D. B., Pilkey, O. H., eds., Shelf Sediment Transport: Process and Pattern. Dowden, Hutchinson and Ross, Stroudsburg, Penn.. 499–574

Tchernia, P., 1980. Descriptive Regional Oceanography. Marine Series 3. Pergamon Press, Oxford. 253

Todd, B. J., 2005. Morphology and Composition of Submarine Barchan Dunes on the Scotian Shelf, Canadian Atlantic Margin. *Geomorphology*, 67: 487–500

Todd, B. J., Fader, G. B. J., Courtney, R. C., et al., 1999. Quaternary Geology and Surficial Sediment Processes, Browns Bank, Scotian Shelf, Based on Multibeam Bathymetry. *Mar. Geol.*, 162: 165–214

Trowbridge, J. H., 1995. A Mechanism for the Formation and Maintenance of Shore-Oblique Sand Ridges on Storm-Dominated Shelves. *Journal of Geophysical Research*, 100: 16071–16086

Venditti, J. C., Bauer, B. O., 2005. Turbulent Flow over a Dune: Green River, Colorado. *Earth Surface Processes and Landforms*, 30: 289–304

Wang, L. J., Sarnthein, M., Erlenkeuser, H., et al., 1999. East Asian Monsoon Climate during the Late Pleistocene: High-Resolution Sediment Records from the South China Sea. *Mar. Geol.*, 156: 245–284

Wang, P. X., 1999. Response of Western Pacific Marginal Seas to Glacial Cycles: Paleoceanographic and Sedimentological Features. *Mar. Geol.*, 156: 5–39

Wang, P. X., Wang, L. J., Bian, Y. H., et al., 1995. Late Quaternary Paleoceanography of the South China Sea: Surface Circulation and Carbonate Cycles. *Mar. Geol.*, 127: 145–165

Wang, S. Y., Gu, Y. Y., Guo, C. Z., 1990. Estuarine Engineering Modals. Ocean Press, Beijing. 120 (in Chinese with English Abstract)

Webster, P., 1987. The Elementary Monsoon. John Wiley & Sons, New York. 3–32

Yan, P., Deng, H., Liu, H., et al., 2006. The Temporal and Spatial Distribution of Volcanism in the South China Sea Region. *Journal of Asian Earth Sciences*, 27: 647–659

Yim, W. W. S., 1999. Radiocarbon Dating and the Reconstruction of Late Quaternary Sea-Level Changes in Hong Kong. *Quaternary International*, 55: 77–91

Yim, W. W. S., Huang, G., Fontugne, M. R., et al., 2006. Postglacial Sea-Level Changes in the Northern South China Sea Continental Shelf: Evidence for a Post-8200 Calendar yr BP Meltwater Pulse. *Quaternary International*, 145–146: 55–67

Zhang, X. Y., Zhang, F. Y., Zhang, W. Y., 2003. Regional Variation of $^{87}Sr/^{86}Sr$ Ratio and Compositions of the Surface Sediment in the Eastern South China Sea. *Acta Oceanologica Sinica*, 25(4): 43–49 (in Chinese with English Abstract)